Gradient Elasticity Theory for Mode III Fracture in Functionally Graded Materials—Part I: Crack Perpendicular to the Material Gradation

G. H. Paulino
Department of Civil and Environmental Engineering, University of Illinois, Newmark Laboratory, 205 North Mathews Avenue, Urbana, IL 61801
Mem. ASME

A. C. Fannjiang
Department of Mathematics, University of California, Davis, CA 95616

Y.-S. Chan
Computer Science and Mathematics Division, Oak Ridge National Laboratory, Oak Ridge, TN 37831

Anisotropic strain gradient elasticity theory is applied to the solution of a mode III crack in a functionally graded material. The theory possesses two material characteristic lengths, ℓ and ℓ', which describe the size scale effect resulting from the underlining microstructure, and are associated to volumetric and surface strain energy, respectively. The governing differential equation of the problem is derived assuming that the shear modulus is a function of the Cartesian coordinate y, i.e., $G=G(y)=G_0e^{\gamma y}$, where G_0 and γ are material constants. The crack boundary value problem is solved by means of Fourier transforms and the hypersingular integrodifferential equation method. The integral equation is discretized using the collocation method and a Chebyshev polynomial expansion. Formulas for stress intensity factors, K_{III}, are derived, and numerical results of K_{III} for various combinations of ℓ, ℓ', and γ are provided. Finally, conclusions are inferred and potential extensions of this work are discussed. [DOI: 10.1115/1.1532321]

1 Introduction

Classical (local) continuum theories possess no intrinsic length scale. Typical dimensions of length are generally associated with the overall geometry of the domain under consideration. Thus classical elasticity and plasticity are scale-free continuum theories in which there is no microstructure associated with material points, [1]. In contrast, strain gradient theories enrich the classical continuum with additional material characteristic lengths in order to describe the size (or scale) effects resulting from the underlining microstructures. Recent work on strain gradient theories to account for size (or scale) effects in materials can be found in the articles by Wu [2], Fleck and Hutchinson [3], Lakes [4,5], Smyshlyaev and Fleck [6], and Van Vliet and Van Mier [7]. Recent applications of gradient elasticity to fracture mechanics include the work by Fannjiang et al. [8], Paulino et al. [9], Exadaktylos et al. [10], Vardoulakis et al. [11], Aifantis [12], Zhang et al. [13], Hwang et al. [14], and the review paper by Hutchinson and Evans [15]. The present work focuses on anisotropic strain gradient elasticity theory for fracture problems in functionally graded materials (FGMs). To the best of the authors' knowledge, this is the first (or one of the first) solutions for FGMs with gradient terms.

The emergence of FGMs is the outcome of the need to accommodate material exposure to nonuniform service requirements. These multiphased materials feature gradual transition in composition and/or microstructure for the specific purpose of controlling variations in thermal, structural, or functional properties. The spatial variation of microstructure is accomplished through nonuniform distribution of the reinforcement phase with different properties, sizes, and shapes, as well as by interchanging the roles of reinforcement and matrix (base) materials in a continuous manner. This concept is illustrated by Fig. 1, which shows an FGM with a continuously graded microstructure. Typical examples of FGMs include ceramic/ceramic (e.g., $MoSi_2$/SiC [16] and TiC/SiC [17]), and metal/ceramic (e.g., Nb/Nb_5Si_3 [18] and Ti/TiB [19]), systems. Comprehensive reviews on several aspects of FGMs can be found in the articles by Markworth et al. [20], Erdogan [21], and Hirai [22], and in the book by Suresh and Mortensen [23].

This paper presents a linkage between gradient elasticity and graded materials within the framework of fracture mechanics. The remainder of the paper is organized as follows. First, the constitutive equations of anisotropic gradient elasticity for nonhomogeneous materials subjected to antiplane shear deformation are given. Then, the governing partial differential equations (PDEs)

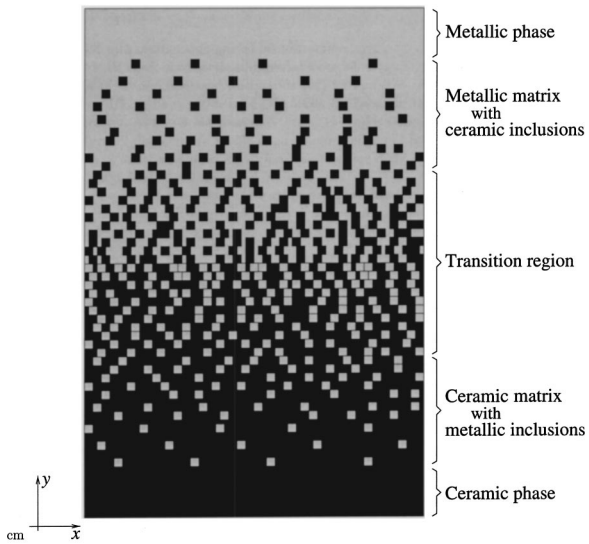

Fig. 1 Functionally graded material (FGM) with continuously graded microstructure

Contributed by the Applied Mechanics Division of THE AMERICAN SOCIETY OF MECHANICAL ENGINEERS for publication in the ASME JOURNAL OF APPLIED MECHANICS. Manuscript received by the ASME Applied Mechanics Division, Oct. 18, 2000; final revision, Sept. 6, 2001. Associate Editor: B. M. Moran. Discussion on the paper should be addressed to the Editor, Prof. Robert M. McMeeking, Department of Mechanical and Environmental Engineering University of California–Santa Barbara, Santa Barbara, CA 93106-5070, and will be accepted until four months after final publication of the paper itself in the ASME JOURNAL OF APPLIED MECHANICS.

are derived and the Fourier transform method is introduced and applied to convert the governing PDE into an ordinary differential equation (ODE). Afterwards, the crack boundary value problem is described and a specific complete set of boundary conditions is given. The governing hypersingular integrodifferential equation is derived and discretized using the collocation method. Next, various relevant aspects of the numerical discretization are described in detail. Subsequently, numerical results are given, conclusions are inferred, and potential extensions of this work are discussed. Two appendices supplement the paper. One contains the lengthy expression of the regular kernel in the final (governing) hypersingular integrodifferential equation, and the other provides some useful formulas for evaluating hypersingular integrals and computing stress intensity factors (SIFs).

2 Constitutive Equations of Gradient Elasticity

This section introduces the notation and constitutive equations of gradient elasticity, which will be used to investigate antiplane shear cracks in functionally graded materials (FGMs). In three-dimensional space, the displacement components are defined as

$$u_x \equiv u, \quad u_y \equiv v, \quad u_z \equiv w, \tag{1}$$

and for antiplane shear problems, the following relations hold:

$$u = v = 0, \quad w = w(x,y). \tag{2}$$

Strains are defined as

$$\epsilon_{ij} = \frac{1}{2}\left(\frac{\partial u_i}{\partial x_j} + \frac{\partial u_j}{\partial x_i} \right), \tag{3}$$

where both the indices i and j run through $(x_1, x_2, x_3) = (x,y,z)$. For antiplane shear problems, the nontrivial strains are

$$\epsilon_{xz} = \frac{1}{2}\frac{\partial w}{\partial x}, \quad \epsilon_{yz} = \frac{1}{2}\frac{\partial w}{\partial y}. \tag{4}$$

Casal [24–26] has established the connection between surface tension effects and anisotropic gradient elasticity theory. For a material graded in the y-direction, the Casal's continuum can be extended so that the strain-energy density has the following form

$$\mathcal{W} = \tfrac{1}{2}\lambda(y)\epsilon_{ii}\epsilon_{jj} + G(y)\epsilon_{ij}\epsilon_{ji} + G(y)\ell^2(\partial_k \epsilon_{ij})(\partial_k \epsilon_{ji}) + \ell' \nu_k \partial_k [G(y)\epsilon_{ij}\epsilon_{ji}], \quad \ell > 0, \tag{5}$$

which has been generalized for an FGM with Lamé moduli $\lambda \equiv \lambda(y)$ and $G \equiv G(y)$. Moreover, $\partial_k = \partial/\partial x_k$. When the formulation is derived by means of a variational principle (or principle of virtual work), terms associated with ℓ undertake a volume integral, and terms associated with ℓ' can be reduced to a surface integral using the divergence theorem. In this sense, the characteristic length ℓ is responsible for volumetric strain-gradient terms, and the characteristic ℓ' is responsible for surface strain-gradient terms. Moreover, ν_k, $\partial_k \nu_k = 0$, is a director field equal to the unit outer normal n_k on the boundaries.

The Cauchy stresses τ_{ij}, the couple stresses μ_{kij} and the total stresses σ_{ij} are defined as

$$\tau_{ij} = \partial \mathcal{W}/\partial \epsilon_{ij} \tag{6}$$

$$\mu_{kij} = \partial \mathcal{W}/\partial \epsilon_{ij,k} \tag{7}$$

$$\sigma_{ij} = \tau_{ij} - \partial_k \mu_{kij}. \tag{8}$$

For homogeneous materials (i.e., λ and G constants), the stress fields are expressed in terms of strains and strain derivatives as

$$\sigma_{ij} = \lambda \epsilon_{kk}\delta_{ij} + 2G(\epsilon_{ij} - \ell^2 \nabla^2 \epsilon_{ij}) \tag{9}$$

$$\tau_{ij} = \lambda \epsilon_{kk}\delta_{ij} + 2G\epsilon_{ij} + 2G\ell' \nu_k \partial_k \epsilon_{ij} \tag{10}$$

$$\mu_{kij} = 2G(\ell' \nu_k \epsilon_{ij} + \ell^2 \partial_k \epsilon_{ij}). \tag{11}$$

As pointed out by Chan et al. [27], the constitutive equations of gradient elasticity for FGMs have a different form from the ones above. Thus, for FGMs with material gradation along the Cartesian coordinate y, the constitutive equations of gradient elasticity are

$$\sigma_{ij} = \lambda(y)\epsilon_{kk}\delta_{ij} + 2G(y)(\epsilon_{ij} - \ell^2 \nabla^2 \epsilon_{ij}) - 2\ell^2 [\partial_k G(y)](\partial_k \epsilon_{ij}) \tag{12}$$

$$\tau_{ij} = \lambda(y)\epsilon_{kk}\delta_{ij} + 2G(y)\epsilon_{ij} + 2\ell' \nu_k [\epsilon_{ij}\partial_k G(y) + G(y)\partial_k \epsilon_{ij}] \tag{13}$$

$$\mu_{kij} = 2\ell' \nu_k G(y)\epsilon_{ij} + 2\ell^2 G(y)\partial_k \epsilon_{ij}. \tag{14}$$

Note that the Cauchy stresses τ_{ij} are influenced by a term containing the spatial derivative of the shear modulus, and so are the total stresses σ_{ij}. The term "$-2\ell^2[\partial_k G(y)](\partial_k \epsilon_{ij})$" that appear in (12), but not in (9), can be interpreted as the interaction between the material gradation and the nonlocal strain gradient effect, which will play a role in the governing partial differential equation (PDE) (17) discussed in the next section. Moreover, if λ and G are constants, the constitutive equations for homogeneous materials (see Vardoulakis et al. [11], Exadaktylos et al. [10], and Fannjiang et al. [8]) are recovered as a particular case of Eqs. (12)–(14). If the shear modulus G is a function of y (see Fig. 2) and a mode III problem is under consideration, then each component of the stress field can be written as, [27]:

$$\begin{aligned} &\sigma_{xx} = \sigma_{yy} = \sigma_{zz} = 0, \quad \sigma_{xy} = 0 \\ &\sigma_{xz} = 2G(y)(\epsilon_{xz} - \ell^2 \nabla^2 \epsilon_{xz}) - 2\ell^2 [\partial_y G(y)](\partial_y \epsilon_{xz}) \neq 0 \\ &\sigma_{yz} = 2G(y)(\epsilon_{yz} - \ell^2 \nabla^2 \epsilon_{yz}) - 2\ell^2 [\partial_y G(y)](\partial_y \epsilon_{yz}) \neq 0 \\ &\mu_{xxz} = 2G(y)\ell^2 \partial_x \epsilon_{xz} \\ &\mu_{xyz} = 2G(y)\ell^2 \partial_x \epsilon_{yz} \end{aligned} \tag{15}$$

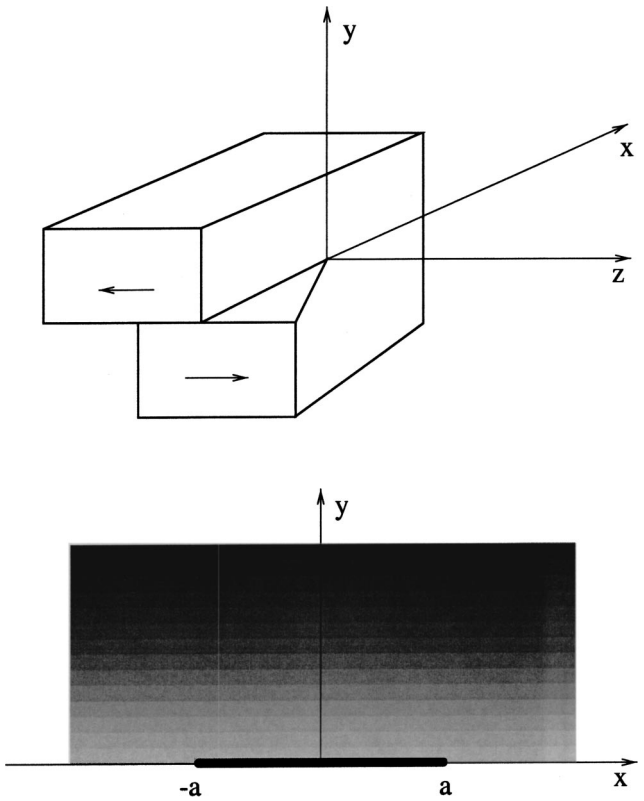

Fig. 2 Mode III crack in a functionally graded material

$$\mu_{yxz}=2G(y)(\ell^2\partial_y\epsilon_{xz}-\ell'\epsilon_{xz})$$
$$\mu_{yyz}=2G(y)(\ell^2\partial_y\epsilon_{yz}-\ell'\epsilon_{yz}).$$

Again, it is worth pointing out that there is an extra term in σ_{xz} and σ_{yz} as compared to the homogeneous material case (see Vardoulakis et al. [11] p. 4534).

3 Governing Partial Differential Equation

By imposing the only nontrivial equilibrium equation

$$\frac{\partial\sigma_{xz}}{\partial x}+\frac{\partial\sigma_{yz}}{\partial y}=0, \tag{16}$$

the following partial differential equation (PDE) for general form of $G(y)$ is obtained:

$$\frac{\partial}{\partial x}\left[G(y)\left(\frac{\partial w}{\partial x}-\ell^2\nabla^2\frac{\partial w}{\partial x}\right)\right]+\frac{\partial}{\partial y}\left[G(y)\left(\frac{\partial w}{\partial y}-\ell^2\nabla^2\frac{\partial w}{\partial y}\right)\right]$$
$$-\ell^2\left[\frac{\partial^2G(y)}{\partial y^2}\frac{\partial^2w}{\partial y^2}+\frac{\partial G(y)}{\partial y}\frac{\partial^3w}{\partial y^3}+\frac{\partial G(y)}{\partial y}\frac{\partial^3w}{\partial x^2\partial y}\right]=0. \tag{17}$$

If the shear modulus G is an exponential function of y, i.e.,

$$G\equiv G(y)=G_0e^{\gamma y}, \tag{18}$$

then (17) can be simplified as

$$-\ell^2\nabla^4w-2\gamma\ell^2\nabla^2\frac{\partial w}{\partial y}+\nabla^2w-\gamma^2\ell^2\frac{\partial^2w}{\partial y^2}+\gamma\frac{\partial w}{\partial y}=0, \tag{19}$$

or in a factored form

$$\left(1-\gamma\ell^2\frac{\partial}{\partial y}-\ell^2\nabla^2\right)\left(\nabla^2+\gamma\frac{\partial}{\partial y}\right)w=0. \tag{20}$$

In terms of the differential operator notation, (20) can be written in the form as

$$\mathsf{H}_\gamma\mathsf{L}_\gamma w=0;\quad \mathsf{H}_\gamma=1-\gamma\ell^2\frac{\partial}{\partial y}-\ell^2\nabla^2,\quad \mathsf{L}_\gamma=\nabla^2+\gamma\frac{\partial}{\partial y}, \tag{21}$$

where H_γ is the perturbed Helmholtz operator, L_γ is the perturbed Laplacian operator, and the two operators commute, i.e., $\mathsf{H}_\gamma\mathsf{L}_\gamma=\mathsf{L}_\gamma\mathsf{H}_\gamma$. Thus, the PDE (20) can be considered as a double perturbation of the composition of the Helmholtz and harmonic equations,

$$(1-\ell^2\nabla^2)\nabla^2w=0, \tag{22}$$

that is, one perturbation is to the Helmholtz operator $(1-\ell^2\nabla^2)$, and the other perturbation is to the Laplacian operator ∇^2. Both the Helmholtz and the Laplacian operators are invariant under "rigid-body motions." However, FGMs bring in the perturbation and destroy such invariance. By setting $\gamma\to0$ in (20), one gets (22), which is the PDE for gradient elasticity.

Another viewpoint of the perturbation is focused on the role of the characteristic length ℓ. By taking $\ell\to0$ (at the level of the differential equation), we obtain a lower order of PDE,

$$\left(\nabla^2+\gamma\frac{\partial}{\partial y}\right)w=0,$$

i.e., the perturbed harmonic equation, which has been investigated by Erdogan and Ozturk [28]. However, because the corresponding term to the coefficient ℓ^2 affects the highest differential in the governing PDE (19), a singular perturbation is expected as the limit $\ell\to0$ is considered. By taking both $\gamma\to0$ and $\ell\to0$, we obtain the harmonic equation for classical elasticity. Various combination of parameters ℓ and γ with the corresponding governing PDE are listed in Table 1.

Table 1 Governing partial differential equations (PDEs) in antiplane shear problems

Cases	Governing PDE	References
$\ell=0,\ \gamma=0$	Laplace equation: $\nabla^2w=0$	Standard textbooks.
$\ell=0,\ \gamma\neq0$	Perturbed Laplace equation: $\left(\nabla^2+\gamma\frac{\partial}{\partial y}\right)w=0$	Erdogan and Ozturk [28].
$\ell\neq0,\ \gamma=0$	Helmholtz-Laplace equation: $(1-\ell^2\nabla^2)\nabla^2w=0$	Vardoulakis *et al.* [11]. Fannjiang *et al.* [8].
$\ell\neq0,\ \gamma\neq0$	Equation (20): $\left(1-\gamma\ell^2\frac{\partial}{\partial y}-\ell^2\nabla^2\right)\left(\nabla^2+\gamma\frac{\partial}{\partial y}\right)w=0$	Studied in this paper.

4 Fourier Transform

Let the Fourier transform be defined by

$$\mathcal{F}(w)(\xi)=W(\xi)=\frac{1}{\sqrt{2\pi}}\int_{-\infty}^{\infty}w(x)e^{ix\xi}dx. \tag{23}$$

The inverse Fourier transform theorem gives

$$\mathcal{F}^{-1}(W)(x)=w(x)=\frac{1}{\sqrt{2\pi}}\int_{-\infty}^{\infty}W(\xi)e^{-ix\xi}d\xi, \tag{24}$$

where $i=\sqrt{-1}$. Now let us assume that

$$w(x,y)=\frac{1}{\sqrt{2\pi}}\int_{-\infty}^{\infty}W(\xi,y)e^{-ix\xi}d\xi, \tag{25}$$

i.e., $w(x,y)$ is the inverse Fourier transform of the function $W(\xi,y)$.

Considering each term in Eq. (17) term by term, and using Eq. (25), one obtains

$$-\ell^2\nabla^4w=-\ell^2\left(\frac{\partial^4w(x,y)}{\partial x^4}+2\frac{\partial^4w(x,y)}{\partial x^2\partial y^2}+\frac{\partial^4w(x,y)}{\partial y^4}\right)$$
$$=\frac{-\ell^2}{\sqrt{2\pi}}\int_{-\infty}^{\infty}\left(\xi^4W(\xi,y)-2\xi^2\frac{\partial^2W}{\partial y^2}+\frac{\partial^4W}{\partial y^4}\right)e^{-ix\xi}\ d\xi \tag{26}$$

$$-2\gamma\ell^2\nabla^2\frac{\partial w}{\partial y}=-2\gamma\ell^2\left(\frac{\partial^3w(x,y)}{\partial x^2\partial y}+\frac{\partial^3w(x,y)}{\partial y^3}\right)$$
$$=-2\frac{\gamma\ell^2}{\sqrt{2\pi}}\int_{-\infty}^{\infty}\left(-\xi^2\frac{\partial W(\xi,y)}{\partial y}+\frac{\partial^3W}{\partial y^3}\right)e^{-ix\xi}\ d\xi \tag{27}$$

$$\nabla^2w=\frac{\partial^2w(x,y)}{\partial x^2}+\frac{\partial^2w(x,y)}{\partial y^2}$$
$$=\frac{1}{\sqrt{2\pi}}\int_{-\infty}^{\infty}\left(-\xi^2W(\xi,y)+\frac{\partial^2W}{\partial y^2}\right)e^{-ix\xi}\ d\xi \tag{28}$$

$$-\gamma^2\ell^2\frac{\partial^2w(x,y)}{\partial y^2}=-\frac{\gamma^2\ell^2}{\sqrt{2\pi}}\int_{-\infty}^{\infty}\frac{\partial^2W(\xi,y)}{\partial y^2}e^{-ix\xi}\ d\xi \tag{29}$$

$$\gamma\frac{\partial w(x,y)}{\partial y}=\frac{\gamma}{\sqrt{2\pi}}\int_{-\infty}^{\infty}\frac{\partial W(\xi,y)}{\partial y}e^{-ix\xi}\ d\xi. \tag{30}$$

Equations (26) to (30) are added (according to Eq. (19)), and after simplification, the governing ordinary differential equation (ODE) is obtained:

$$\left[\ell^2\frac{d^4}{dy^4}+2\gamma\ell^2\frac{d^3}{dy^3}-(2\ell^2\xi^2+\gamma^2\ell^2+1)\frac{d^2}{dy^2}-\gamma(1+2\ell^2\xi^2)\frac{d}{dy}\right.$$
$$\left.+(\ell^2\xi^4+\xi^2)\right]W=0. \tag{31}$$

Table 2 Roots λ_i together with corresponding mechanics theory and type of material

Cases	Number of roots	Roots	Mechanics theory and type of material	References
$\ell=0,\ \gamma=0$	2	$\pm\lvert\xi\rvert$	Classical LEFM, homogeneous materials	Standard textbooks.
$\ell=0,\ \gamma\neq 0$	2	$-\gamma/2\pm\sqrt{\gamma^2/4+\xi^2}$	Classical LEFM, nonhomogeneous materials	Erdogan and Ozturk [28].
$\ell\neq 0,\ \gamma=0$	4	$\pm\lvert\xi\rvert,\ \pm\sqrt{\xi^2+1/\ell^2}$	Gradient theories, homogeneous materials	Vardoulakis *et al.* [11]. Fannjiang *et al.* [8].
$\ell\neq 0,\ \gamma\neq 0$	4	$-\gamma/2\pm\sqrt{\gamma^2/4+\xi^2}$, $-\gamma/2\pm\sqrt{\xi^2+\gamma^2/4+1/\ell^2}$	Gradient theories, nonhomogeneous materials	Studied in this paper.

5 Solutions of the Ordinary Differential Equation

The corresponding characteristic equation to the ordinary differential equation (ODE) (31) is

$$\ell^2\lambda^4+2\gamma\ell^2\lambda^3-(2\ell^2\xi^2+\gamma^2\ell^2+1)\lambda^2-\gamma(1+2\ell^2\xi^2)\lambda+(\ell^2\xi^4+\xi^2)=0, \tag{32}$$

which can be further factored as

$$[\ell^2\lambda^2+\gamma\ell^2\lambda-(1+\ell^2\xi^2)](\lambda^2+\gamma\lambda-\xi^2)=0. \tag{33}$$

Clearly the four roots λ_i $(i=1,2,3,4)$ of the polynomial (33) above can be obtained as

$$\lambda_1=\frac{-\gamma}{2}-\frac{\sqrt{\gamma^2+4\xi^2}}{2},\quad \lambda_2=\frac{-\gamma}{2}+\frac{\sqrt{\gamma^2+4\xi^2}}{2}, \tag{34}$$

$$\lambda_3=\frac{-\gamma}{2}-\sqrt{\xi^2+\gamma^2/4+1/\ell^2},\quad \lambda_4=\frac{-\gamma}{2}+\sqrt{\xi^2+\gamma^2/4+1/\ell^2}, \tag{35}$$

where we let $\lambda_1<0$ and $\lambda_3<0$. As $\gamma\to 0$, we recover the roots found by Vardoulakis et al. [11] and Fannjiang et al. [8]. The roots λ_1 and λ_2 correspond to the solution of the perturbed harmonic equation, and the roots λ_3 and λ_4 match with the solution of the perturbed Helmholtz's equation. Various choices of parameters ℓ and γ with their corresponding mechanics theories and material types are listed in Table 2.

By taking account of the far-field boundary condition

$$w(x,y)\to 0\ \text{ as }\ \sqrt{x^2+y^2}\to+\infty, \tag{36}$$

and with $y>0$ (the upper half plane), one obtains

$$W(\xi,y)=A(\xi)e^{\lambda_1 y}+B(\xi)e^{\lambda_3 y}. \tag{37}$$

Accordingly, the displacement $w(x,y)$ takes the form

$$w(x,y)=\frac{1}{\sqrt{2\pi}}\int_{-\infty}^{\infty}[A(\xi)e^{\lambda_1 y}+B(\xi)e^{\lambda_3 y}]e^{-ix\xi}d\xi. \tag{38}$$

Both $A(\xi)$ and $B(\xi)$ are determined by the boundary conditions.

6 Boundary Conditions

Figure 2 shows the geometry of the mode III crack problem in which a functionally graded material (FGM), with shear modulus $G(y)=G_0e^{\gamma y}$, bonded to a half-space is considered. Thus the problem reduces to the upper half-plane, and $y=0$ is treated as the boundary. By the principle of virtual work, the following mixed boundary conditions can be derived:

$$\begin{cases}\sigma_{yz}(x,0)=p(x), & |x|<a\\ w(x,0)=0, & |x|>a\\ \mu_{yyz}(x,0)=0, & -\infty<x<+\infty,\end{cases} \tag{39}$$

which are adopted in this paper. One may observe that the first two boundary conditions (BCs) in (39) are from classical elasticity, e.g., linear elastic fracture mechanics (LEFM). The last BC regarding the couple-stress μ_{yyz} is needed as the higher order theory is considered.

7 Hypersingular Integrodifferential Equation Approach

By taking account of the symmetry along the x-axis, we may consider that $w(x,y)$ takes the following general solution form (for the upper half-plane):

$$\begin{aligned}w(x,y)&=\frac{1}{\sqrt{2\pi}}\int_{-\infty}^{\infty}[A(\xi)e^{\lambda_1 y}+B(\xi)e^{\lambda_3 y}]e^{-ix\xi}d\xi,\quad y\geqslant 0\\ &=\frac{1}{\sqrt{2\pi}}\int_{-\infty}^{\infty}[A(\xi)e^{-(\gamma+\sqrt{4\xi^2+\gamma^2})y/2}\\ &\quad+B(\xi)e^{-(\gamma+\sqrt{4\xi^2+\gamma^2+4/\ell^2})y/2}]e^{-ix\xi}d\xi,\quad y\geqslant 0,\end{aligned} \tag{40}$$

where $A(\xi)$ and $B(\xi)$ need to be determined from the boundary conditions (39). As Eq. (40) provides the form of the solution for $w(x,y)$, it can be used in conjunction with Eq. (15) such that

$$\begin{aligned}\sigma_{yz}(x,y)&=2G(y)(\epsilon_{yz}-\ell^2\nabla^2\epsilon_{yz})-2\ell^2[\partial_y G(y)](\partial_y\epsilon_{yz})\\ &=\frac{G(y)}{\sqrt{2\pi}}\int_{-\infty}^{\infty}\lambda_1(\gamma,\xi)A(\xi)e^{-(\gamma+\sqrt{\gamma^2+4\xi^2})y/2-ix\xi}d\xi,\\ &\quad y\geqslant 0.\end{aligned} \tag{41}$$

Notice that the term associated with $B(\xi)$ has been dropped out from $\sigma_{yz}(x,y)$. Moreover,

$$\begin{aligned}\mu_{yyz}(x,y)&=2G(y)\left(\ell^2\frac{\partial\epsilon_{yz}}{\partial y}-\ell'\epsilon_{yz}\right),\quad y\geqslant 0,\\ &=\frac{G(y)}{\sqrt{2\pi}}\int_{-\infty}^{\infty}\{(\ell^2\lambda_1^2-\ell'\lambda_1)A(\xi)e^{\lambda_1 y}+(\ell^2\lambda_3^2\\ &\quad-\ell'\lambda_3)B(\xi)e^{\lambda_3 y}\}e^{-ix\xi}d\xi\\ &=\frac{G(y)}{\sqrt{2\pi}}\int_{-\infty}^{\infty}\{c_A(\gamma,\xi)A(\xi)e^{-(\gamma+\sqrt{\gamma^2+4\xi^2})y/2}\\ &\quad+c_B(\gamma,\xi)B(\xi)e^{-(\gamma+\sqrt{4\xi^2+\gamma^2+4/\ell^2})y/2}\}e^{-ix\xi}d\xi,\end{aligned} \tag{42}$$

where

$$c_A(\gamma,\xi)=\ell^2\lambda_1^2-\ell'\lambda_1$$
$$=\frac{\gamma}{2}(\gamma\ell^2+\ell')+\frac{1}{2}(\gamma\ell^2+\ell')\sqrt{\gamma^2+4\xi^2}+\ell^2\xi^2, \tag{43}$$

and

$$c_B(\gamma,\xi)=\ell^2\lambda_3^2-\ell'\lambda_3$$
$$=\ell^2\xi^2+\frac{\gamma}{2}(\gamma\ell^2+\ell')+1$$
$$+\frac{1}{2}(\gamma\ell^2+\ell')\sqrt{4\xi^2+\gamma^2+4/\ell^2}. \tag{44}$$

In order to derive the Fredholm integral equation, we define the density as the slope function

$$\phi(x)=\partial w(x,0^+)/\partial x. \tag{45}$$

The second boundary condition in (39), and Eq. (45), imply that

$$\phi(x)=0, \quad |x|>a, \tag{46}$$

and

$$\int_{-a}^{a}\phi(x)dx=0, \tag{47}$$

which is the single-valuedness condition. The definition (45), together with Eq. (40), lead to

$$\frac{1}{\sqrt{2\pi}}\int_{-\infty}^{\infty}(-i\xi)[A(\xi)+B(\xi)]e^{-ix\xi}d\xi=\phi(x), \quad -\infty<x<\infty. \tag{48}$$

By inverting the Fourier transform and using (46), one obtains

$$(i\xi)[A(\xi)+B(\xi)]=\frac{-1}{\sqrt{2\pi}}\int_{-\infty}^{\infty}\phi(x)e^{ix\xi}dx, \quad -\infty<x<\infty$$
$$=\frac{-1}{\sqrt{2\pi}}\int_{-a}^{a}\phi(t)e^{i\xi t}dt. \tag{49}$$

The last boundary condition in (39), imposed on $\mu_{yyz}(x,y)$, provides the following pointwise relationship between $A(\xi)$ and $B(\xi)$:

$$B(\xi)=-\frac{\ell^2\xi^2+(\gamma\ell^2+\ell')\sqrt{\gamma^2/4+\xi^2}+\gamma(\gamma\ell^2+\ell')/2}{\ell^2\xi^2+1+[(\gamma\ell^2+\ell')/2](\gamma+\sqrt{4\xi^2+\gamma^2+4/\ell^2})}A(\xi)$$
$$=\rho(\gamma,\xi)A(\xi), \tag{50}$$

where the notation $\rho(\gamma,\xi)$ is introduced here, i.e.,

$$\rho(\gamma,\xi)=-\frac{\ell^2\xi^2+(\gamma\ell^2+\ell')\sqrt{\gamma^2/4+\xi^2}+\gamma(\gamma\ell^2+\ell')/2}{\ell^2\xi^2+1+[(\gamma\ell^2+\ell')/2](\gamma+\sqrt{4\xi^2+\gamma^2+4/\ell^2})}. \tag{51}$$

Substituting (50) into (49), one obtains

$$A(\xi)=\frac{-1}{\sqrt{2\pi}i\xi}\left[\frac{1}{1+\rho(\gamma,\xi)}\right]\int_{-a}^{a}\phi(t)e^{i\xi t}dt, \tag{52}$$

where

$$\frac{1}{1+\rho(\gamma,\xi)}=\frac{\ell^2\xi^2+1+[(\gamma\ell^2+\ell')/2](\gamma+\sqrt{4\xi^2+\gamma^2+4/\ell^2})}{1+[(\gamma\ell^2+\ell')/2](\sqrt{4\xi^2+\gamma^2+4/\ell^2}-\sqrt{4\xi^2+\gamma^2})}. \tag{53}$$

Replacing $A(\xi)$ in Eq. (41) and using the (first) boundary condition for σ_{yz} (that is, $\lim_{y\to0^+}\sigma_{yz}(x,y)=p(x)$, $|x|<a$) in (39), one obtains the following integral equation in limit form:

$$\lim_{y\to0^+}\frac{G(y)}{2\pi}\int_{-\infty}^{\infty}\left[\frac{-\lambda_1(\gamma,\xi)}{i\xi(1+\rho(\gamma,\xi))}\right]$$
$$\times\left[\int_{-a}^{a}\phi(t)e^{i\xi t}dt\right]e^{-(\gamma+\sqrt{\gamma^2+4\xi^2})y/2-ix\xi}d\xi$$
$$=p(x), \quad |x|<a. \tag{54}$$

By rearranging the order of integration, we obtain

$$\lim_{y\to0^+}\frac{G(y)}{2\pi}\int_{-a}^{a}\phi(t)\int_{-\infty}^{\infty}\frac{-\lambda_1(\gamma,\xi)}{(i\xi)[1+\rho(\gamma,\xi)]}$$
$$\times e^{-(\gamma+\sqrt{\gamma^2+4\xi^2})y/2}e^{i\xi(t-x)}d\xi dt$$
$$=p(x), \quad |x|<a, \tag{55}$$

which can be rewritten as

$$\lim_{y\to0^+}\frac{G}{2\pi}\int_{-a}^{a}\phi(t)\int_{-\infty}^{\infty}K(\xi,y)e^{i\xi(t-x)}d\xi dt=p(x), \quad |x|<a, \tag{56}$$

with the kernel

$$K(\xi,y)=\frac{-\lambda_1(\gamma,\xi)}{i\xi[1+\rho(\gamma,\xi)]}e^{-(\gamma+\sqrt{\gamma^2+4\xi^2})y/2}. \tag{57}$$

Asymptotic analysis allows splitting of the kernel $K(\xi,y)$ into the singular $[K_\infty(\xi,y)=\lim_{|\xi|\to\infty}K(\xi,y)]$ and nonsingular parts:

$$K(\xi,y)=\underbrace{K_\infty(\xi,y)}_{\text{singular}}+\underbrace{[K(\xi,y)-K_\infty(\xi,y)]}_{\text{nonsingular}}, \tag{58}$$

where (as y is set to zero)

$$K_\infty(\xi,0)=\frac{|\xi|}{i\xi}\left\{\left[\frac{5\ell^2\gamma^2}{8}+\frac{\ell'\gamma}{4}+1-\left(\frac{\ell'}{2l}\right)^2\right]\right.$$
$$\left.+\frac{2\gamma\ell^2+\ell'}{2}|\xi|+\ell^2\xi^2\right\}, \tag{59}$$

and $K(\xi,0)-K_\infty(\xi,0)$, denoted by $N(\xi,0)=N(\xi)$, can be expressed as a fraction:

$$N(\xi,0)=N(\xi)=\frac{P(\xi)}{Q(\xi)}, \tag{60}$$

with $P(\xi)$ and $Q(\xi)$ described in Appendix A.

Substitution of Eq. (59) into (56), in the sense of distribution theory, [29], leads to

$$\lim_{y\to0^+}\int_{-\infty}^{\infty}K_\infty(\xi,y)e^{i\xi(t-x)}d\xi$$
$$=\frac{-2\ell^2}{(t-x)^3}-\frac{\pi}{2}(2\ell^2\gamma+\ell')\delta'(t-x)$$
$$+\frac{5\ell^2\gamma^2/8+\ell'\gamma/4+1-[\ell'/(2\ell)]^2}{t-x},$$

and to the following hypersingular integral equation:

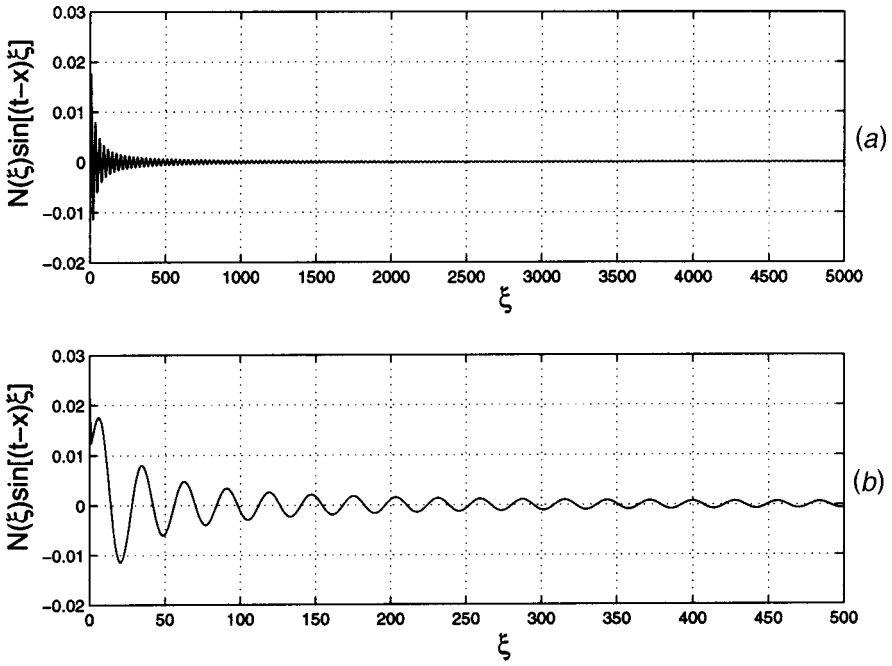

Fig. 3 Plot of the integrand in Eq. (62) for $\ell=0.05$, $\ell'=0.005$, $\gamma=0.1$, $r=\sqrt{3}/7$, and $s=\sqrt{2}/3$. (*a*) $\xi\in[0,5000]$; (*b*) Zoom for the range $\xi\in[0,500]$. Moreover, as $\xi\to 0$, the limit of $N(\xi)\sin[\xi(s-r)]$ is about 22.4×10^{-3}.

$$\frac{G_0}{\pi}\Xint=_{-a}^{a}\left\{\frac{-2\ell^2}{(t-x)^3}-\frac{\pi}{2}(2\ell^2\gamma+\ell')\delta'(t-x)+\frac{5\ell^2\gamma^2/8+\ell'\gamma/4+1-[\ell'/(2\ell)]^2}{t-x}+k(x,t)\right\}\phi(t)dt=p(x),\quad |x|<a, \tag{61}$$

where the regular kernel is

$$k(x,t)=\int_0^\infty N(\xi)\sin[\xi(t-x)]d\xi \tag{62}$$

with $N(\xi)$ described in Eq. (60). Figure 3 permits to graphically evaluate the behavior of the integrand of Eq. (62). Clearly, such kernel is oscillatory, but the magnitude of oscillation decreases and tend to zero as ξ increases, i.e., $\lim_{\xi\to\infty}N(\xi)\sin[\xi(t-x)]=0$. Another point that we need to be cautious about in Eq. (62) is the behavior at $\xi=0$ of $N(\xi)=P(\xi)/Q(\xi)$ as $Q(\xi)$ has the factor ξ in the denominator. However, this would not affect the integrability of the integrand in Eq. (62) because of the term $\sin[\xi(t-x)]$. Thus $\lim_{\xi\to 0}N(\xi)\sin[\xi(t-x)]$ exists and is finite, which depends on the values of t, x, ℓ, ℓ', and γ.

As a result of distribution theory, [29], the differentiation of a delta function, $\delta(t)$, has the following property:

$$\int_{-\infty}^{\infty}\delta'(t-x)\phi(t)dt=-\phi'(x). \tag{63}$$

Thus one may rewrite Eq. (61) as

$$\frac{G_0}{\pi}\Xint=_{-a}^{a}\left\{\frac{-2\ell^2}{(t-x)^3}+\frac{5\ell^2\gamma^2/8+\ell'\gamma/4+1-(\ell'/\ell)^2/4}{t-x}+k(x,t)\right\}\times\phi(t)dt+\frac{G}{2}(\ell'+2\ell^2\gamma)\phi'(x)=p(x),\quad |x|<a, \tag{64}$$

which is an integrodifferential equation with both hypersingular and Cauchy singular kernels. In addition to the single-valuedness condition condition in (47), the integrodifferential Eq. (64) is solved under the physical constraint ("smooth closure condition"):

$$\phi(a)=\phi(-a)=0, \tag{65}$$

so that the solution can be found uniquely (see Refs. [8] and [30]).

8 Numerical Solution

The numerical solution of the mode III fracture boundary value problem is accomplished by means of the collocation method, [31,32]. The process of obtaining the numerical solution of Eq. (64) can be divided into the following steps:

- Normalization,
- representation of the density function,
- Chebyshev polynomial expansion,
- evaluation of the derivative of the density function,
- formation of the linear system of equations,
- evaluation of singular and hypersingular integrals, and
- evaluation of nonsingular integral.

Relevant details for each of the above items are given below.

8.1 Normalization. By the following change of variables,

$$s=[2/(d-c)][t-(c+d)/2],$$

one may convert the integral $\int_c^d g(t)dt$ into the form of $\int_{-1}^{1}f(s)ds$. Because the crack surface is located in the range $(-a,a)$, a convenient change of variables becomes

$$t/a=s\quad\text{and}\quad x/a=r,$$

which is the normalization of the variables t and x, respectively. Thus Eq. (64) can be written in normalized fashion as

$$\frac{1}{\pi}\oint\!\!\!\!\!\!=\int_{-1}^{1}\left\{\frac{-2(\ell/a)^2}{(s-r)^3}+\frac{5(\ell/a)^2(a\gamma)^2/8+(\ell'/a)(a\gamma)/4+1-[(\ell'/a)/(\ell/a)]^2/4}{s-r}+\mathcal{K}(r,s)\right\}\Phi(s)ds+[\ell'/a+2(\ell/a)^2(a\gamma)]\Phi'(r)/2=\mathcal{P}(r)/G_0,\quad |r|<1, \tag{66}$$

where

$$\Phi(r)=\phi(ar),\quad \mathcal{P}(r)=p(ar),\quad \mathcal{K}(r,s)=ak(ar,as).$$

As clearly seen in Eq. (66), the quantities ℓ/a, ℓ'/a, and $a\gamma$ are dimensionless parameters. Thus the following dimensionless parameters are defined:

$$\tilde{\ell}=\ell/a,\quad \tilde{\ell}'=\ell'/a,\quad \tilde{\gamma}=a\gamma, \tag{67}$$

which will be used in the numerical implementation and results.

8.2 Representation of the Density Function. The next step of the numerical approach to the (normalized) hypersingular integral Eq. (66) is to establish the actual behavior of the unknown density function $\Phi(s)$ around the two crack tips $s=\pm 1$. For example, the governing integral equation in classical linear elastic fracture mechanics (LEFM) has Cauchy singularity if the slope function, say $\Phi(s)_{\mathrm{LEFM}}$, is chosen to be the unknown density function. A well-known representation is, [31,32],

$$\Phi(s)_{\mathrm{LEFM}}=f(s)/\sqrt{1-s^2},\quad |s|<1,$$

where $f(\pm 1)\neq 0$. For the cubic hypersingular integral, Eq. (66), the representation of $\Phi(s)$ is found to be, [8],

$$\Phi(s)_{\mathrm{GE}}\equiv\Phi(s)=g(s)\sqrt{1-s^2}, \tag{68}$$

where $g(\pm 1)$ is finite, $g(\pm 1)\neq 0$, and the subscript GE stands for gradient elasticity. Thus by approximating $g(s)$, one can find the numerical solution to $\Phi(s)$.

8.3 Chebyshev Polynomial Expansion. The approximation of $g(s)$ in Eq. (68) is accomplished by means of Chebyshev polynomial expansions. Either Chebyshev polynomials of the first kind $T_n(s)$, or of the second kind $U_n(s)$, may be employed in the approximation, i.e.,

$$g(s)=\sum_{n=0}^{\infty}a_nT_n(s)\quad\text{or}\quad g(s)=\sum_{n=0}^{\infty}A_nU_n(s). \tag{69}$$

The coefficients a_ns or A_ns are determined numerically by the collocation method. As shown by Chan et al. [33], the two expansions should lead to the same numerical results. In this paper, the expansion using $U_n(s)$ is adopted, i.e.,

$$\Phi(s)=\sqrt{1-s^2}\sum_{n=0}^{\infty}A_nU_n(s), \tag{70}$$

where $U_n(s)$ is defined, as usual, by

$$U_n(s)=\frac{\sin[(n+1)\cos^{-1}(s)]}{\sin[\cos^{-1}(s)]},\quad n=0,1,2,\ldots. \tag{71}$$

Satisfaction of the single-valuedness condition (47), or equivalently, $\int_{-1}^{1}\Phi(s)\,ds=0$, requires that the following relation holds:

$$A_0=0. \tag{72}$$

8.4 Evaluation of the Derivative of the Density Function. The term $\Phi'(r)$ in Eq. (66) is evaluated using the expansion (70) and the fact that

$$\frac{d}{dr}[U_n(r)\sqrt{1-r^2}]=-\frac{n+1}{\sqrt{1-r^2}}T_{n+1}(r),\quad n\geq 0. \tag{73}$$

Thus

$$\Phi'(r)=\frac{d}{dr}\left[\sqrt{1-r^2}\sum_{n=0}^{\infty}A_nU_n(r)\right]=\frac{-1}{\sqrt{1-r^2}}\sum_{n=0}^{\infty}(n+1)A_nT_n(r). \tag{74}$$

8.5 Formation of the Linear System of Equations. The strategy to determine the coefficients A_ns consists of forming a set of linear algebraic equations. Replacing $\Phi(s)$ in (66) by the representation (70), and using (74) one obtains the governing integral equation in discretized form:

$$-2\tilde{\ell}^2\sum_{n=1}^{\infty}\frac{A_n}{\pi}\oint\!\!\!\!\!\!=\int_{-1}^{1}\frac{U_n(s)\sqrt{1-s^2}}{(s-r)^3}ds+\left[1+\frac{5\tilde{\ell}^2\tilde{\gamma}^2}{8}+\frac{\tilde{\ell}'\tilde{\gamma}}{4}-\left(\frac{\tilde{\ell}'}{2\tilde{\ell}}\right)^2\right]\sum_{n=1}^{\infty}\frac{A_n}{\pi}\oint\!\!\!\!\!\!=\int_{-1}^{1}\frac{U_n(s)\sqrt{1-s^2}}{s-r}ds+\sum_{n=1}^{\infty}\frac{A_n}{\pi}\int_{-1}^{1}\sqrt{1-s^2}U_n(s)\mathcal{K}(r,s)ds-\frac{\tilde{\ell}'+2\tilde{\ell}^2\tilde{\gamma}}{2\sqrt{1-r^2}}\sum_{n=1}^{\infty}A_n(n+1)T_{n+1}(r)=\frac{\mathcal{P}(r)}{G_0},\quad |r|<1. \tag{75}$$

Notice that the running index n starts from 1 instead of 0 (see (72)).

8.6 Evaluation of Singular and Hypersingular Integrals. The governing integrodifferential Eq. (64), and its discretized version, Eq. (75), contain both Cauchy singular and hypersingular integrals (cubic singularity), which need to be evaluated. Erdogan et al. [31,32] have presented formulas for evaluating Cauchy singular integrals, and Chan et al. [34] have presented formulas for evaluating a broad class of hypersingular integrals, which generalizes previous derivations, [31,32,35], in the literature. Here, such integrals are interpreted in the finite-part sense, and listed in Appendix B (Eq. (93) to (95)).

8.7 Evaluation of Nonsingular Integral. Combining all the results obtained so far in the numerical approximation, one may rewrite Eq. (75) in the following form:

$$\frac{-\tilde{\ell}^2}{2(1-r^2)}\sum_{n=1}^{\infty}A_n[(n^2+n)U_{n+1}(r)-(2n^2+3n+2)U_{n-1}(r)]-\left[1+\frac{5\tilde{\ell}^2\tilde{\gamma}^2}{8}+\frac{\tilde{\ell}'\tilde{\gamma}}{4}-\left(\frac{\tilde{\ell}'}{2\tilde{\ell}}\right)^2\right]\sum_{n=1}^{\infty}A_nT_{n+1}(r)+\sum_{n=1}^{\infty}\frac{A_n}{\pi}\int_{-1}^{1}\sqrt{1-s^2}U_n(s)\mathcal{K}(r,s)ds-\frac{\tilde{\ell}'+2\tilde{\ell}^2\tilde{\gamma}}{2\sqrt{1-r^2}}\sum_{n=1}^{\infty}A_n(n+1)T_{n+1}(r)=\frac{\mathcal{P}(r)}{G},\quad |r|<1. \tag{76}$$

Thus the last step for applying the collocation method consists of evaluating the (regular) integral in (76), which is actually a double integral, i.e.,

$$\int_{-1}^{1}\sqrt{1-s^2}U_n(s)\mathcal{K}(r,s)ds$$

$$=\int_{-1}^{1}\sqrt{1-s^2}U_n(s)ak(ar,as)ds$$

$$=\int_{-1}^{1}\sqrt{1-s^2}U_n(s)\int_0^{\infty}aN(\xi)\sin[a\xi(s-r)]d\xi ds.$$

The integral along $[0,\infty)$ is a Fourier sine transform, and can be efficiently evaluated by applying fast Fourier transform (FFT) [36]. The integral along $[-1,1]$ can be readily obtained by the Gaussian quadrature method, [37].

9 Stress Intensity Factors (SIFs)

Since the (macroscopic) propagation of a crack starts around its tips, it is very important to study and determine the SIFs at both crack tips. In classical linear elastic fracture mechanics (LEFM), the stress $\sigma_{yz}(x,0)$ has $1/\sqrt{x-a}$ singularity as $x\to a^+$ (or $1/\sqrt{x+a}$, as $x\to -a^-$), and thus SIFs are defined and can be calculated by

$$K_{\mathrm{III}}(a)=\lim_{x\to a^+}\sqrt{2\pi(x-a)}\sigma_{yz}(x,0),\quad (x>a), \tag{77}$$

and

$$K_{\mathrm{III}}(-a)=\lim_{x\to -a^-}\sqrt{2\pi(-a-x)}\sigma_{yz}(x,0),\quad (x<-a). \tag{78}$$

However, the same definition may not hold for strain-gradient elasticity because $\sigma_{yz}(x,0)$ may have a stronger singularity, [13]. Thus SIFs will be redefined in the development below.

First, note that the limit in Eqs. (77) and (78) is taken from the region outside the crack surfaces toward both tips, and the integral Eq. (64) is the expression for $\sigma_{yz}(x,0)$ which is valid for $|x|>a$ as well as $|x|<a$, i.e.,

$$\sigma_{yz}(x,0)=\frac{G}{\pi}\int_{-a}^{a}\left\{\frac{-2\ell^2}{(t-x)^3}+\frac{5\ell^2\gamma^2/8+\ell'\gamma/4+1-(\ell'/\ell)^2/4}{t-x}+k(x,t)\right\}\phi(t)dt+\frac{G}{2}(\ell'+2\ell^2\gamma)\phi'(x),\quad |x|>a. \tag{79}$$

Second, after normalization and with the density function $\Phi(t)$ expanded by Chebyshev polynomials of the second kind U_n, some integral formulas, which are useful for deriving SIFs, need to be developed for $|r|>1$ (Chan et al. [34]), and are listed in Appendix B (see Eqs. (96) to (98)). Notice that the highest singularity in the Eqs. (96) to (98) appears in the last term in Eq. (98), and it has singularity $(r^2-1)^{-3/2}$ as $r\to 1^+$ or $r\to -1^-$. Motivated by such asymptotic behavior, we generalize the SIFs for strain gradient elasticity from those of classical LEFM. Thus

$$\ell K_{\mathrm{III}}(a)=\lim_{x\to a^+}2\sqrt{2\pi(x-a)}(x-a)\ \sigma_{yz}(x,0), \tag{80}$$

$$\ell K_{\mathrm{III}}(-a)=\lim_{x\to -a^-}2\sqrt{2\pi(x+a)}(x+a)\sigma_{yz}(x,0). \tag{81}$$

Therefore, the following formulas for the normalized mode III SIFs in the strain-gradient elasticity theory may be derived:

$$\ell K_{\mathrm{III}}(a)=\lim_{x\to a^+}2\sqrt{2\pi(x-a)}(x-a)\sigma_{yz}(x,0),\quad (x>a)$$

$$=\lim_{r\to 1^+}2\sqrt{2\pi(ar-a)}(ar-a)\sigma_{yz}(ar,0),\quad (r>1)$$

$$=2a\sqrt{\pi a}\ G_0\lim_{r\to 1^+}\sqrt{2(r-1)}(r-1)\frac{-2\ell^2}{\pi a^2}$$

$$\times\int_{-1}^{1}\frac{\Phi(s)}{(s-r)^3}ds,\quad (r>1). \tag{82}$$

After cancellation of the common terms, Eq. (82) can be continued by introducing formula (98), and using the representation (70), i.e.,

$$K_{\mathrm{III}}(a)=2\sqrt{2\pi a}\left(\frac{-2\ell}{a}\right)G_0\lim_{r\to 1^+}(r-1)^{3/2}\sum_{n=0}^{N}\frac{-(n+1)}{2}\times\left(r-\frac{|r|}{r}\sqrt{r^2-1}\right)^{n-1}\left[n\left(1-\frac{|r|}{\sqrt{r^2-1}}\right)^2+\frac{r-\frac{|r|}{r}\sqrt{r^2-1}}{\sqrt{r^2-1^3}}\right]A_n$$

$$=\sqrt{\pi a}\ (\ell/a)G_0\sum_{n=0}^{\infty}(n+1)A_n. \tag{83}$$

Similarly,

$$K_{\mathrm{III}}(-a)=\sqrt{\pi a}\ (\ell/a)G_0\sum_{n=0}^{\infty}(-1)^n(n+1)A_n. \tag{84}$$

Formulas (83) and (84) will be used to obtain numerical results for SIFs.

10 Results and Discussion

The boundary value problem illustrated in Fig. 2 is considered for all the examples in this paper. To validate the present formulation, consider the case where $\ell,\ \ell'\to 0$ in a certain special limit sense (see Fannjiang et al. [8]), so that the classical elasticity solution is represented. The results for classical stress intensity factors (SIFs) (Eqs. (77) and (78)) are given in Table 3. It is clearly seen from Table 3 that the present results are in agreement with those of Erdogan and Ozturk [28]. Note that the SIFs decrease monotonically as γ increases. Moreover, it is interesting to investigate the asymptotic behavior of the SIFs as $\gamma\to\pm\infty$. As $\gamma\to\infty$ the stiffness of the medium increases indefinitely and, under finite loading (p_0), the crack-opening displacement and the SIFs $K_{\mathrm{III}}(a)$ tend to zero. Similarly, as $\gamma\to-\infty$ the stiffness of the

Table 3 Variation of classical (normalized) stress intensity factors (SIFs) with the material gradation parameter $\tilde{\gamma}=\gamma/a$

	$\frac{K_{III}(-a)}{p_0\sqrt{\pi a}}$	
$\tilde{\gamma}$	Present Study	Erdogan and Ozturk [28]
-2.0	1.476	1.481
-1.6	1.381	1.397
-1.2	1.293	1.308
-0.8	1.204	1.214
-0.4	1.117	1.113
-0.2	1.061	1.059
0.0	1.000	1.000
0.2	0.934	0.934
0.4	0.866	0.869
0.6	0.807	0.810
0.8	0.755	0.758
1.0	0.709	0.712
1.2	0.669	0.671
1.6	0.602	0.604
2.0	0.556	0.550
3.0	0.458	0.457
5.0	0.359	0.356
6.0	0.329	0.324

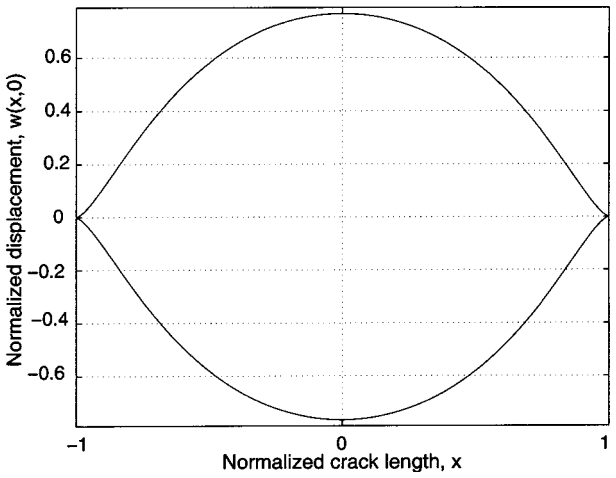

Fig. 4 Full crack displacement profile in an infinite medium of homogeneous material ($\tilde{\gamma}=0$) under uniform crack surface shear loading $\sigma_{yz}(x,0)=-p_0$ with choice of (normalized) $\tilde{\ell}=0.2$ and $\tilde{\ell}'=0$

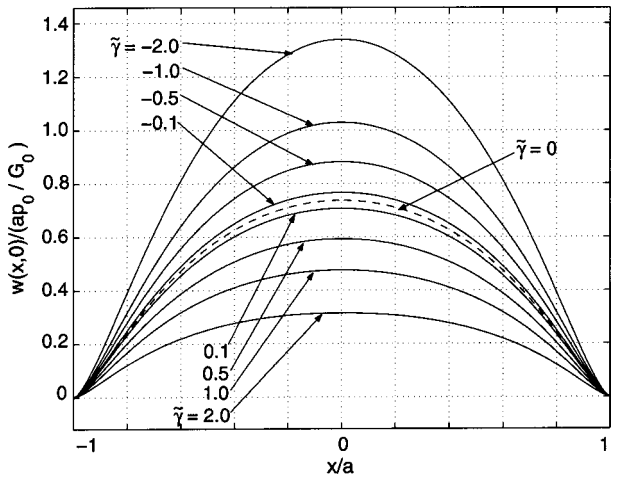

Fig. 6 Crack surface displacement under uniform crack surface shear loading $\sigma_{yz}(x,0)=-p_0$ and shear modulus $G(y)=G_0e^{\gamma y}$ with choice of (normalized) $\tilde{\ell}=0.2$, $\tilde{\ell}'=0.04$, and various $\tilde{\gamma}$. The dashed line stands for the homogeneous material ($\tilde{\gamma}=0$) in a gradient elastic medium.

medium decreases indefinitely, and consequently $K_{\mathrm{III}}(a)$ tend to infinity. These physically expected trends can be observed in Table 3.

Once the slope function is found numerically using the representation (68), the crack displacement profile $w(r,0)$ can be obtained as

$$w(r,0)=\int_{-1}^{r}\Phi(s)ds=\int_{-1}^{r}\sqrt{1-s^2}\sum_{n=0}^{N}A_nU_n(s)ds. \quad (85)$$

Figure 4 shows the normalized crack displacement profile in an infinite medium of homogeneous material ($\gamma=0$) under uniform crack surface loading for $\tilde{\ell}=0.2$ and $\tilde{\ell}'=0$. Notice that the crack tips form a cusp with zero enclosed angle and zero first derivative of the displacement at the crack tips (see (65)). This crack shape is similar to the one obtained by Barenblatt [38] using "cohesive zone theory," but without the assumption regarding existence of interatomic forces.

The solutions obtained in this study for a nonhomogeneous half-plane having shear modulus $G\equiv G(y)$, $y>0$, is also valid for the corresponding infinite medium in which $y=0$ is a plane of symmetry (see Fig. 2), i.e.,

$$G(-y)=G(y).$$

Unless otherwise stated, uniform loading is considered on the crack face, i.e., $\sigma_{yz}(x,0)=-p_0$, and the normalization p_0/G_0 has been employed.

Further normalized crack displacement profiles for various combinations of the gradient parameters $(\tilde{\ell},\tilde{\ell}')$ and material gradation parameter $(\tilde{\gamma})$ are presented in Fig. 5 to Fig. 8. Figures 5 and 6 show crack displacement profiles for selected values of $\tilde{\ell}$, $\tilde{\ell}'$, and various γ. Figure 5 considers $\tilde{\ell}=0.05$, $\tilde{\ell}'=0$ and thus $\rho=\ell'/\ell=0$; while Fig. 6 considers $\tilde{\ell}=0.20$, $\tilde{\ell}'=0.04$ and thus $\rho=\ell'/\ell=0.2$. In both graphs, the broken lines stand for the homogeneous material ($\gamma=0$) in a gradient elastic medium. A com-

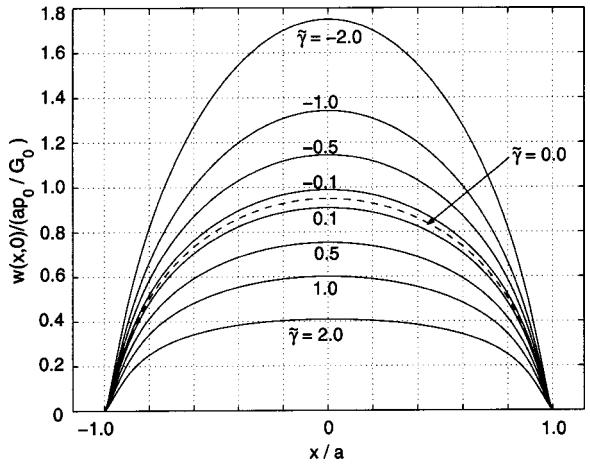

Fig. 5 Crack surface displacement under uniform crack surface shear loading $\sigma_{yz}(x,0)=-p_0$ and shear modulus $G(y)=G_0e^{\gamma y}$ with choice of (normalized) $\tilde{\ell}=0.05$, $\tilde{\ell}'=0$, and various $\tilde{\gamma}$. The dashed line stands for the homogeneous material case ($\tilde{\gamma}=0$).

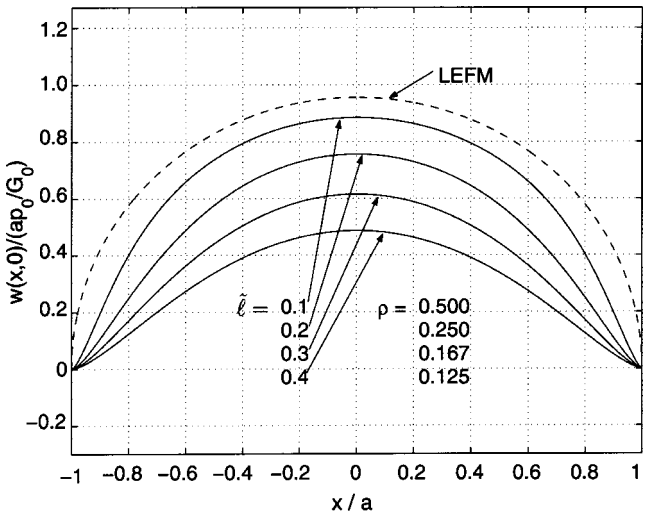

Fig. 7 Crack surface displacement profiles under uniform crack surface shear loading $\sigma_{yz}(x,0)=-p_0$ and shear modulus $G(y)=G_0e^{\gamma y}$ with choice of (normalized) $\tilde{\ell}'=0.05$, $\tilde{\gamma}=0.1$, and various $\tilde{\ell}$. The values of $\tilde{\ell}$ are listed in the same order as the solid-line curves.

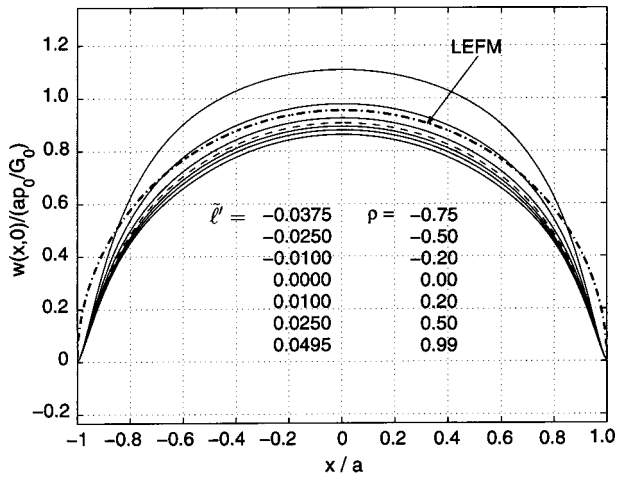

Fig. 8 Crack surface displacement profiles under uniform crack surface shear loading $\sigma_{yz}(x,0)=-p_0$ and shear modulus $G(y)=G_0e^{\gamma y}$ with choice of (normalized) $\tilde{\ell}=0.05$, $\tilde{\gamma}=0.1$, and various $\tilde{\ell}'$. The values of $\tilde{\ell}'$ (and $\rho=\ell/\ell'$) are listed in the same order as the solid-line and dashed-line ($\rho=0$) curves representing the strain gradient results.

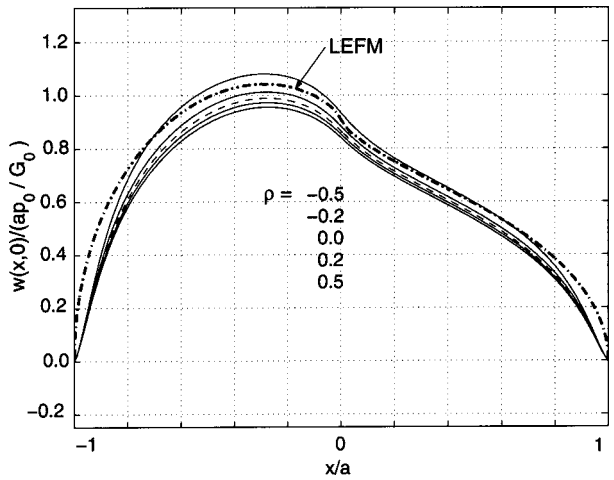

Fig. 9 Crack surface displacement profiles under discontinuous loading $p(x/a)=-1+0.5\ \mathrm{sgn}(x/a)$ and shear modulus $G(y)=G_0e^{\gamma y}$ with choice of (normalized) $\tilde{\ell}=0.05$, $\tilde{\gamma}=0.2$, and various $\rho=\ell/\ell'$. The values of ρ are listed in the same order as the solid-line and dashed-line ($\rho=0$) curves representing the strain gradient results.

parison between Figs. 5 and 6 permits to assess the influence of the gradient parameters (ℓ,ℓ') on the displacement solution. Moreover, as γ increases the displacement magnitude decreases, which is consistent with similar results by Erdogan and Ozturk [28] using classical elasticity to model mode III cracks in functionally graded materials (FGMs).

Figure 7 shows crack displacement profiles for $\tilde{\ell}'=0.05$, $\tilde{\gamma}=0.10$ and various $\tilde{\ell}$. As $\tilde{\ell}$ increases, the displacement diminishes monotonically, or alternatively the crack becomes stiffer, in comparison to the classical elasticity theory.

Figure 8 shows crack displacement profiles for $\tilde{\ell}=0.05$, $\tilde{\gamma}=0.10$ and various $\tilde{\ell}'$. As is apparent from this figure, by maintaining the values of the relative volume energy parameter $\tilde{\ell}$ constant, the crack stiffening effect becomes more pronounced as the relative surface energy parameter $\tilde{\ell}'$ increases in the range $[0,\tilde{\ell})$. It is worth mentioning that, from energy considerations, the parameter $\tilde{\ell}'$ can take negative values, [39]. Note from Fig. 8 that the effect of a negative $\tilde{\ell}'$ leads to a more compliant crack. In general, this is a desirable property of the mathematical model in regards to describing experimental results and data.

Table 4 Convergence of (normalized) generalized stress intensity factors (SIFs) for a mode III crack

	$\tilde{\gamma}=0,\ \tilde{\ell}=0.05$				$\tilde{\gamma}=0.30,\ \tilde{\ell}=0.05$			
	$\tilde{\ell}'=0;\ \rho=0$		$\tilde{\ell}'=0.01;\ \rho=0.20$		$\tilde{\ell}'=0;\ \rho=0$		$\tilde{\ell}'=0.01;\ \rho=0.20$	
N	$\frac{K_{III}(-a)}{p_0\sqrt{\pi a}}$	Cond. Num.	$\frac{K_{III}(-a)}{p_0\sqrt{\pi a}}$	Cond. Num.	$\frac{K_{III}(-a)}{p_0\sqrt{\pi a}}$	Cond. Num.	$\frac{K_{III}(-a)}{p_0\sqrt{\pi a}}$	Cond. Num.
11	0.97292	9.888	0.99640	17.018	0.89258	15.223	0.90773	15.142
21	0.97467	83.559	0.97375	1.669e+02	0.88381	1.509e+02	0.88337	1.478e+02
31	0.97467	3.555e+02	0.97355	7.131e+02	0.88376	6.437e+02	0.88287	6.314e+02
41	0.97467	1.032e+03	0.972256	2.059e+03	0.88336	1.859e+03	0.88133	1.823e+03
51	0.97467	2.395e+03	0.97109	4.754e+03	0.88301	4.293e+03	0.87999	4.206e+03
61	0.97467	4.802e+03	0.97113	9.501e+03	0.88301	8.577e+03	0.87996	8.406e+03

Table 5 Normalized generalized stress intensity factors (SIFs) for a mode III crack at various values of $\tilde{l}$, $\tilde{l}'$, and $\tilde{\gamma}$

	$\tilde{\ell}=0.05,\ \tilde{\ell}'=0$	$\tilde{\ell}=0.05,\ \tilde{\ell}'=0.01$	$\tilde{\ell}=0.2,\ \tilde{\ell}'=0$	$\tilde{\ell}=0.2,\ \tilde{\ell}'=0.04$
$\tilde{\gamma}$	$\frac{K_{III}(-a)}{p_0\sqrt{\pi a}}$	$\frac{K_{III}(-a)}{p_0\sqrt{\pi a}}$	$\frac{K_{III}(-a)}{p_0\sqrt{\pi a}}$	$\frac{K_{III}(-a)}{p_0\sqrt{\pi a}}$
-2.00	1.42126	1.41617	1.28917	1.26783
-1.00	1.21749	1.21301	1.10392	1.08610
-0.50	1.10374	1.09965	1.00377	0.98768
-0.10	1.00271	0.99903	0.91696	0.90236
0.00	0.97467	0.97113	0.89338	0.87921
0.10	0.94423	0.94086	0.86819	0.85450
0.50	0.82566	0.82282	0.76878	0.75671
1.00	0.70597	0.70324	0.66261	0.65169
2.00	0.54916	0.54592	0.50894	0.49937

Figure 9 shows crack displacement profiles considering discontinuous loading

$$p(x) = -1 + 0.5\,\mathrm{sgn}(x)$$

and $\tilde{\ell} = 0.05$, $\tilde{\gamma} = 0.2$, and various $\rho = \ell'/\ell$. Similar comments to those regarding Fig. 8 can be made with respect to Fig. 9. Moreover, qualitatively the results displayed in Figs. 7 to 9 are in agreement with those of Vardoulakis et al. [11] for homogeneous materials.

Table 4 shows a convergence study for (normalized) generalized SIFs (see Eqs. (80), (81), and (83), (84)) involving nongraded ($\tilde{\gamma} = 0$) and graded ($\tilde{\gamma} \neq 0$) gradient elastic materials considering both $\tilde{\ell}' = 0$ and $\tilde{\ell}' \neq 0$ ($\tilde{\ell}' > 0$). Note that as the number of collocation points (N) increases, the generalized SIF results converge for both materials (i.e., nongraded and graded). However, the convergence is worse for the case $\tilde{\ell}' \neq 0$ than for the case $\tilde{\ell}' = 0$. The condition number for all the examples investigated is always satisfactory.

Table 5 lists the generalized SIFs (see Eqs. (80), (81)) for gradient elastic materials considering various values of the material parameter γ and using $N = 61$ collocation points in the numerical solution. Notice that the SIF monotonically decreases as γ increases, which is in full agreement with the early results for classical elasticity considering nonhomogeneous materials (see Table 3). Consider, for example, the case $\tilde{\gamma} = 0$. In this case, the crack stiffening is due to the characteristic material lengths $\tilde{\ell}$ and $\tilde{\ell}'$ ($\tilde{\ell}' > 0$) of the structured medium which are responsible for lower generalized SIFs (< 1.0) and, consequently, lower energy release rates during crack propagation. The results indicate that a higher external load, as compared to that of the classical case, must be applied on the crack surfaces (or on the remote boundaries) to propagate it in a material with microstructure.

A few comments about the determination of characteristic lengths in continua with microstructure are in order. Shi et al. [40] have presented a brief discussion on determination of such lengths in the context of Fleck and Hutchinson's [3] strain gradient theory, which is a generalization of Mindlin's higher-order continuum theory, [41,42]. Experimental work in the field include, for example, micro-torsion by Fleck et al. [43], microbending by Stolkens and Evans [44], and microindentation by Nix [45]. The characterization of actual materials, with respect to strain gradient length-scale(s), is an ongoing research topic of much interest and impact in the field of applied mechanics.

11 Concluding Remarks

This paper has presented a theoretical framework and corresponding computational implementation for modeling antiplane shear cracks in functionally graded materials (FGMs) using strain gradient elasticity (Casal's continuum), which includes both volumetric and surface energy terms. The characteristic lengths (ℓ and ℓ', respectively) associated to these terms are assumed to be constant, and the material shear modulus is assumed to vary exponentially (see Eq. (18)). In this study, the crack is considered to be perpendicular to the material gradient. The present hypersingular integrodifferential equation approach leads to a numerically tractable solution of the fracture problem, and relevant fracture parameters have been investigated. These results include, for example, crack displacement profiles and generalized stress intensity factors. A parametric study including various gradation parameters (γ) and strain gradient parameters ($\tilde{\ell}, \tilde{\ell}'$) has been conducted and discussed. A natural extension of this work is the solution of an antiplane shear crack where the crack is parallel to the material gradation. Another potential extension consists of investigating the mode I fracture problem.

Acknowledgments

We acknowledge the support from the USA National Science Foundation (NSF) through grants CMS-9996378 (previously CMS-9713798) from the Mechanics & Materials Program, and DMS-9600119 from the Applied Mathematics Program. The first author would like to thank Prof. Y. F. Dafalias, form the University of California at Davis, for his encouragement and valuable suggestions to this work.

Appendix A

The Regular Kernel. The regular kernel $N(\xi,0)$ described in Eq. (60) can be expressed as the fraction $P(\xi)/Q(\xi)$. $Q(\xi)$ is given by

$$Q(\xi) = -i\xi\left(\sqrt{\xi^2+\gamma^2/4+1/\ell^2}+\sqrt{\xi^2+\gamma^2/4}+\gamma+\ell'/\ell^2\right). \tag{86}$$

$P(\xi)$ can be expressed as

$$P(\xi) = P_4(\xi)+P_3(\xi)+P_2(\xi)+P_1(\xi)+P_0(\xi) \tag{87}$$

in which

$$P_4(\xi) = \ell^2\xi^2\times\left(\sqrt{\xi^2+\gamma^2/4+1/\ell^2}\sqrt{\xi^2+\gamma^2/4}+\xi^2 - |\xi|\sqrt{\xi^2+\gamma^2/4+1/\ell^2}-|\xi|\sqrt{\xi^2+\gamma^2/4}\right), \tag{88}$$

$$P_3(\xi) = \tfrac{1}{2}\left(\gamma\ell^2+\ell'\right)\xi^2\left(\sqrt{\xi^2+\gamma^2/4+1/\ell^2}+\sqrt{\xi^2+\gamma^2/4}\right) - \left(\gamma\ell^2+\ell'\right)|\xi|^3, \tag{89}$$

$$P_2(\xi) = \left[1+\gamma\left(\gamma\ell^2+\ell'\right)\right]\sqrt{\xi^2+\gamma^2/4+1/\ell^2}\sqrt{\xi^2+\gamma^2/4} + \left[1+\frac{1}{4}\gamma^2\ell^2-\frac{1}{2}\left(\frac{\ell'}{\ell}\right)^2-\frac{1}{2}\gamma\ell'\right]\xi^2 - \left[1+\frac{5}{8}\gamma^2\ell^2-\left(\frac{\ell'}{2\ell}\right)^2+\frac{1}{4}\gamma\ell'\right] \times|\xi|\left(\sqrt{\xi^2+\gamma^2/4+1/\ell^2}+\sqrt{\xi^2+\gamma^2/4}\right), \tag{90}$$

$$P_1(\xi) = \frac{1}{2}\gamma\left(1+\gamma^2\ell^2+\gamma\ell'\right)\sqrt{\xi^2+\gamma^2/4+1/\ell^2} + \left[\frac{\gamma}{2}\left(1+\gamma^2\ell^2+\gamma\ell'\right)+\frac{\ell'}{\ell^2}\right]\sqrt{\xi^2+\gamma^2/4} - \left(\gamma+\frac{\ell'}{\ell^2}\right)\left[1+\frac{5}{8}\gamma^2\ell^2-\left(\frac{\ell'}{2\ell}\right)^2+\frac{1}{4}\gamma\ell'\right]|\xi|, \tag{91}$$

$$P_0(\xi) = \frac{1}{4}\ell^2\gamma^4+\frac{3}{4}\gamma^2+\frac{1}{4}\gamma^3\ell'+\frac{1}{2}\frac{\gamma\ell'}{\ell^2}. \tag{92}$$

Appendix B

Singular and Hypersingular Integrals. Closed-form solutions for evaluating singular and hypersingular integrals are provided here and can also be found in Chan et al. [34]. Those integrals are interpreted in the finite-part sense.

The solution of the crack boundary value problem requires the following formulas. Thus for $|r| < 1$, we have

$$\frac{1}{\pi}\int_{-1}^{1}\frac{U_n(s)\sqrt{1-s^2}}{s-r}\,ds = -T_{n+1}(r), \quad n \geq 0, \tag{93}$$

$$\frac{1}{\pi}\oint\!\!\!\!\!\!-_{-1}^{1}\frac{U_n(s)\sqrt{1-s^2}}{(s-r)^2}\,ds = -(n+1)U_n(r), \quad n \geq 0 \tag{94}$$

$$\frac{1}{\pi}\oint_{-1}^{1}\frac{U_n(s)\sqrt{1-s^2}}{(s-r)^3}ds=\begin{cases}-1, & n=0,\\ [(n^2+n)U_{n+1}(r)-(2n^2+3n+2)U_{n-1}(r)]/[4(1-r^2)], & n\geq 1.\end{cases} \tag{95}$$

The calculation of stress intensity factors requires the following formulas. Thus, for $|r|>1$, we have

$$\frac{1}{\pi}\int_{-1}^{1}\frac{U_n(s)\sqrt{1-s^2}}{s-r}ds=-\left(r-\frac{|r|}{r}\sqrt{r^2-1}\right)^{n+1},\quad n\geq 0 \tag{96}$$

$$\frac{1}{\pi}\int_{-1}^{1}\frac{U_n(s)\sqrt{1-s^2}}{(s-r)^2}ds=-(n+1)\left(1-\frac{|r|}{\sqrt{r^2-1}}\right)\times\left(r-\frac{|r|}{r}\sqrt{r^2-1}\right)^{n},\quad n\geq 0 \tag{97}$$

$$\frac{1}{\pi}\int_{-1}^{1}\frac{U_n(s)\sqrt{1-s^2}}{(s-r)^3}ds=\frac{-1}{2}(n+1)\left(r-\frac{|r|}{r}\sqrt{r^2-1}\right)^{n-1}\times\left[n\left(1-\frac{|r|}{\sqrt{r^2-1}}\right)^2+\frac{r-\frac{|r|}{r}\sqrt{r^2-1}}{\sqrt{r^2-1^3}}\right],\quad n\geq 0. \tag{98}$$

References

[1] Eringen, A. C., 1999, *Microcontinuum Field Theories I. Foundations and Solids*, Springer-Verlag, New York.

[2] Wu, C. H., 1992, "Cohesive Elasticity and Surface Phenomena," Q. Appl. Math., **50**(1), pp. 73–103.

[3] Fleck, N. A., and Hutchinson, J. W., 1997, "Strain Gradient Plasticity," Adv. Appl. Mech., **33**, pp. 295–361.

[4] Lakes, R. S., 1983, "Size Effects and Micromechanics of a Porous Solid," J. Mater. Sci., **18**, pp. 2572–2580.

[5] Lakes, R. S., 1986, "Experimental Microelasticity of Two Porous Solids," Int. J. Solids Struct., **22**, pp. 55–63.

[6] Smyshlyaev, V. P., and Fleck, N. A., 1996, "The Role of Strain Gradients in the Grain Size Effect for Polycrystals," J. Mech. Phys. Solids, **44**(4), pp. 465–495.

[7] Van Vliet, M. R. A., and Van Mier, J. G. M., 1999, "Effect of Strain Gradients on the Size Effect of Concrete in Uniaxial Tension," Int. J. Fract., **95**, pp. 195–219.

[8] Fannjiang, A. C., Chan, Y.-S., and Paulino, G. H., 2001, "Strain Gradient Elasticity for Antiplane Shear Cracks: A Hypersingular Integrodifferential Equation Approach," SIAM (Soc. Ind. Appl. Math.) J. Appl. Math., **62**(3), pp. 1066–1091.

[9] Paulino, G. H., Fannjiang, A. C., and Chan, Y.-S., 1999, "Gradient Elasticity Theory for a Mode III Crack in a Functionally Graded Material," Mater. Sci. Forum, **308–311**, pp. 971–976.

[10] Exadaktylos, G., Vardoulakis, I., and Aifantis, E., 1996, "Cracks in Gradient Elastic Bodies With Surface Energy," Int. J. Fract., **79**(2), pp. 107–119.

[11] Vardoulakis, I., Exadaktylos, G., and Aifantis, E., 1996, "Gradient Elasticity With Surface Energy: Mode-III Crack Problem," Int. J. Solids Struct., **33**(30), pp. 4531–4559.

[12] Aifantis, E., 1992, "On the Role of Gradients in the Localization of Deformation and Fracture," Int. J. Eng. Sci., **30**, pp. 1279–1299.

[13] Zhang, L., Huang, Y., Chen, J. Y., and Hwang, K. C., 1998, "The Mode III Full-Field Solution in Elastic Materials With Strain Gradient Effects," Int. J. Fract., **92**(4), pp. 325–348.

[14] Hwang, K. C., Cuo, T. F., Huang, Y., and Chen, J. Y., 1998, "Fracture in Strain Gradient Elasticity," Met. Mater., **4**(4), pp. 593–600.

[15] Hutchinson, J. W., and Evans, A. G., 2000, "Mechanics of Materials: Top-Down Approaches to Fracture," Acta Mater., **48**, pp. 125–135.

[16] Carrillo-Heian, E. M., Carpenter, R. D., Paulino, G. H., Gibeling, J. C., and Munir, Z. A., 2001, "Dense Layered $MoSi_2$/SiC Functionally Graded Composites Formed by Field-Activated Synthesis," J. Am. Ceram. Soc., **84**(5), pp. 962–968.

[17] Jin, Z.-H., and Paulino, G. H., 2001, "Transient Thermal Stress Analysis of an Edge Crack in a Functionally Graded Material," Int. J. Fract., **107**(1), pp. 73–98.

[18] Carrillo-Heian, E. M., Unuvar, C., Gibeling, J. C., Paulino, G. H., and Munir, Z. A., 2001, "Simultaneous Synthesis and Densification of Niobium Silicide/Niobium Composites," Scr. Mater., **45**(4), pp. 405–412.

[19] Carpenter, R. D., Liang, W. W., Paulino, G. H., Gibeling, J. C., and Munir, Z. A., 1999, "Fracture Testing and Analysis of a Layered Functionally Graded Ti/TiB Beam in 3-Point Bending," Mater. Sci. Forum, **837–842**, pp. 971–976.

[20] Markworth, A. J., Ramesh, K. S., and Parks, Jr., W. P., 1995, "Review Modelling Studies Applied to Functionally Graded Materials," J. Mater. Sci., **30**, pp. 2183–2193.

[21] Erdogan, F., 1995, "Fracture Mechanics of Functionally Graded Materials," Composites Eng., **5**(7), pp. 753–770.

[22] Hirai, T., 1996, "Functional Gradient Materials," *Materials Science and Technology*, (Vol. 17B of *Processing of Ceramics, Part 2*), R. J. Brook, ed., VCH Verlagsgesellschaft mbH, Weinheim, Germany, pp. 292–341.

[23] Suresh, S., and Mortensen, A., 1998, *Fundamentals of Functionally Graded Materials*, ASM International and the Institute of Materials, IOM Communications Ltd., London.

[24] Casal, P., 1961, "La Capillarite Interne," Cah. Groupe Fr. Etud. Rheol., **6**(3), pp. 31–37.

[25] Casal, P., 1963, "Capillarite Interne en Mecanique," C.R. Acad. Sci., **256**, pp. 3820–3822.

[26] Casal, P., 1972, "La théorie du second gradient et la capillarité," C.R. Acad. Sci. Paris Sér. A, **274**, pp. 1571–1574.

[27] Chan, Y.-S., Paulino, G. H., and Fannjiang, A. C., 2003, "Change of Constitutive Relations due to Interaction Between Strain Gradient Effect and Material Gradation," to be submitted.

[28] Erdogan, F., and Ozturk, M., 1992, "Diffusion Problems in Bonded Nonhomogeneous Materials With an Interface Cut," Int. J. Eng. Sci., **30**(10), pp. 1507–1523.

[29] Sneddon, I. N., 1972, *The Use of Integral Transforms*, McGraw-Hill, New York.

[30] Martin, P. A., 1991, "End-Point Behavior of Solutions to Hypersingular Integral Equations," Proc. R. Soc. London, Ser. A, **432**(1885), pp. 301–320.

[31] Erdogan, F., and Gupta, G. D., 1972, "On the Numerical Solution of Singular Integral Equations," Q. Appl. Math., **30**, pp. 525–534.

[32] Erdogan, F., Gupta, G. D., and Cook, T. S., 1973, "Numerical Solution of Singular Integral Equations," *Mechanics of Fracture*, G. C. Sih, Ed., Vol. 1, Noordhoff, Leyden, The Netherlands, pp. 368–425.

[33] Chan, Y.-S., Paulino, G. H., and Fannjiang, A. C., 2001, "The Crack Problem for Nonhomogeneous Materials Under Antiplane Shear Loading—A Displacement Based Formulation," Int. J. Solids Struct., **38**(17), pp. 2989–3005.

[34] Chan, Y.-S., Fannjiang, A. C., and Paulino, G. H., 2003, "Integral Equations With Hypersingular Kernels—Theory and Applications to Fracture Mechanics," Int. J. Eng. Sci., **41**(7), pp. 683–720.

[35] Kaya, A. C., and Erdogan, F., 1987, "On the Solution of Integral Equations With Strongly Singular Kernels," Q. Appl. Math., **45**(1), pp. 105–122.

[36] Folland, G. B., 1992, *Fourier Analysis and Its Applications*, Wadsworth & Brooks/Cole Advanced Books & Software, Pacific Grove, CA.

[37] Stroud, A. H., and Secrest, D., 1996, *Gaussian Qudrature Formulas*, Prentice-Hall, New York.

[38] Barenblatt, G. I., 1962, "The Mathematical Theory of Equilibrium Cracks in Brittle Fracture," Adv. Appl. Mech., **7**, pp. 55–129.

[39] Vardoulakis, I., and Sulem, J., 1995, *Bifurcation Analysis in Geomechanics*, Blackie Academic and Professional, Glasgow.

[40] Shi, M. X., Huang, Y., and Hwang, K. C., 2000, "Fracture in a Higher-Order Elastic Continuum," J. Mech. Phys. Solids, **48**(12), pp. 2513–2538.

[41] Mindlin, R. D., 1964, "Micro-Structure in Linear Elasticity," Arch. Ration. Mech. Anal., **16**, pp. 51–78.

[42] Mindlin, R. D., 1965, "Second Gradient of Strain and Surface-Tension in Linear Elasticity," Int. J. Solids Struct., **1**, pp. 417–438.

[43] Fleck, N. A., Muller, G. M., Asby, M. F., and Hutchinson, J. W., 1994, "Strain Gradient Plasticity: Theory and Experiments," Acta Metall. Mater., **42**, pp. 475–487.

[44] Stolken, J. S., and Evans, A. G., 1998, "A Microbend Test Method for the Plasticity Length Scale," Acta Mater., **46**, pp. 5109–5115.

[45] Nix, W. D., 1997, "Elastic and Plastic Properties of Thin Films on Substrates: Nanoindentation Techniques," Mater. Sci. Eng., A, **234/236**, pp. 37–44.